Proceedings of the International Conference on Oxide Materials for Electronic Engineering (OMEE 2021)

Nanocatalysts for Carbon Monoxide Oxidation Based on Acid Modified Polyphase Aluminosilicate Support and Contained Palladium(II) and Copper(II) Salts

T.O. Kiose[a,b,*], T.L. Rakitskaya[a,b], A.A.-A. Ennan[b] and Yu.I. Popruha[a]

[a] *Faculty of Chemistry and Pharmacy, Odessa I.I. Mechnikov National University, Dvoryanskaya Str. 2, 65082 Odessa, Ukraine*
[b] *Physico-Chemical Institute of Environment and Human' Protection, Preobrazhenskaya Str. 3, 65082 Odessa, Ukraine*

Doi: 10.12693/APhysPolA.141.286 *e-mail: kiosetatyana@gmail.com

Basalt tuff from Rivnes'ka Oblast' (Ukraine) was used as a support ($\bar{S}$) for catalysts containing palladium(II) and copper(II) salts as base components. XRD, FT-IR spectroscopy, and pH-metry were used for the characterization of natural basalt tuff (N-BT), its acid-modified forms, and palladium–copper catalysts based on these supports (K_2PdCl_4–$Cu(NO_3)_2$-KBr/$\bar{S}$). Both natural and chemically modified basalt tuffs contain the following phases: clinoptilolite, mordenite, montmorillonite and also α-quartz and hematite. Crystallite sizes of the phases are in the range of 9 to 90 nm. It has been found that the catalytic activity of the Pd(II)–Cu(II)/3N-BT-0.5 compositions depends not only on the acid treatment duration (its optimal value is 0.5 h) but also on the nature of acids HNO_3, H_3PO_4, H_2SO_4, and $C_6H_8O_7$ (citric acid). Some catalytic compositions are suggested for use in devices intended for respiratory protection against carbon monoxide.

topics: natural and chemically modified basalt tuffs, carbon monoxide, catalysts, oxidation.

1. Introduction

Almost 50 years ago, a Wacker-type catalyst containing $PdCl_2$ and $CuCl_2$, in the form of a homogeneous liquid phase and heterogenized by deposition on porous carriers, was first used for low-temperature oxidation of carbon monoxide by atmospheric oxygen [1, 2]. Despite some achievements in the study of supported metal complex catalysts for the oxidation of CO (SMCC-CO) [3], interest in them has not weakened, and over the past 10 years approximately 20% of publications have been devoted to a detailed study of the influence of various factors on their activity at ambient temperature and increased relative humidity [4].

The analysis shows that the basic components remain salts of palladium(II) and copper(II), and a change in the activity of SMCC-CO is achieved by varying the precursors of Pd(II) and Cu(II) [3, 5–7], the nature of the carrier and a method for applying metal complex compositions. Al_2O_3 [3, 5–8] and activated carbons [5, 6, 9–11] are initially most widely used as carriers. Studies on the effect of pre-acid treatment of AC [10, 12] and Al_2O_3 [13] carriers, mainly HNO_3 and HCl, on the activity of SMCC-CO were not systematic (are episodic in nature) and there was no noticeable increase in the activity of the compositions. Recently, carbon fiber materials [14, 15] and carbon nanotubes (CNT) have been proposed as carriers [16]. Although one of the first attempts [7] to use natural materials, namely, acid-modified mordenite, was unsuccessful (a very low rate of CO oxidation), subsequent studies [17–22] showed the potential of such natural materials as tripoli, clinoptilolite (Cli), mordenite (Mord), bentonite, basalt tuff (BT) and polygorskite. In some cases, a change in the activity of SMCC-CO occurs due to pretreatment of the natural support with thermal and chemical methods, as a result of which its structural, morphological, and physicochemical properties change, affecting the composition of surface palladium-copper complexes and, consequently, their catalytic activity [3].

Since natural materials differ in their genesis (origin), phase composition, and phase ratio in polyphase minerals, in each case, subject to the general approaches of acid modification [23, 24], a systematic study of the effect of carrier pretreatment conditions on the activity of SMCC-CO is necessary [20, 22]. The nature and concentration of the acid, the duration (time) of the acid contacting with the carrier, and the processing temperature [18, 22–25] affect the change in the properties of the carrier most significantly. The experiment

showed that the activity of SMCC-CO does not always increase upon pretreatment of a carrier with an increase in acid concentration and contact time [20, 22]. Basalt tuff as a carrier of palladium(II) and copper(II) salts is described in the study [18]. The carrier was treated with boiling 3M HNO_3 for 3, 6, 9, 12, 15 h. During a three-hour treatment, nitric acid of concentration 3, 6, 8, 10, 12 mol/L was used. Thus, rather stringent conditions for acid modification of basalt tuff were applied. We showed [19, 20] that in the case of clinoptilolite, it is sufficient to subject it to 3M HNO_3 acid treatment for 30 or 60 min to obtain SMCC-CO with maximum activity.

The objective of this work is to optimize the conditions of acid modification of a polyphase natural aluminosilicate — basalt tuff and to establish their effect on the activity of catalysts containing palladium(II) and copper(II) salts in the reaction of low-temperature oxidation of CO with oxygen.

2. Experimental

X-ray phase analysis was carried out using a Siemens D500 (Germany) powder diffractometer in copper radiation (CuK_α, $\lambda = 1.54178$ Å), with a secondary beam graphite monochromator. To record the diffractograms, the test samples were thoroughly grounded in an agate mortar and placed in a glass cuvette with a working volume of $2 \times 1 \times 0.1$ cm^3. Diffractograms were recorded in the range of angles $3° < 2\theta < 70°$ with a step of 0.03° and an accumulation time of 60 s at each point.

Scanning electron microscope (SEM) studies of morphology and determination of local composition were performed by electron probe microanalysis on a scanning electron microscope JSM-6390LV (Japan).

Samples were examined by IR spectroscopy using Perkin Elmer FT-IR Spectrometer Frontier (USA) (400–4000 cm^{-1}, with a resolution of 4 cm^{-1}). The spectra were registered in KBr tablets, which were obtained at a ratio of 1 mg of substance per 200 mg of KBr and compressed under a pressure of 7 t/cm^2 for 30 s.

To characterize protolytic properties of surface functional groups, 0.2 g of natural basalt tuff (N-BT) or acid-modified basalt tuff (H-BT) samples were suspended in 20 mL of bidistilled water, and an equilibrium pH value was measured by a pH-340 instrument equipped with an ESL 43-07 glass electrode and an EVL 1M3 chlorsilver electrode, at continuous stirring of the suspension at 20°C. A suspension effect ΔpH_S was estimated using

$$\Delta pH_S = pH_{st} - pH_0, \tag{1}$$

where pH_0 and pH_{st} are pH values of a suspension measured in 15 s and after the equilibrium attainment, respectively.

In our work, we used samples of N-BT (Ukraine, Transcarpathian region, Polytsky II) with the following average composition: SiO_2 — 63.62; Al_2O_3 — 19.60; Fe_2O_3 — 10.49; MnO — 0.12; TiO_2 — 1.82. The ratio of SiO_2/Al_2O_3 is 3.2, and the specific surface area is 18 m^2/g. Two series of acid-modified samples were obtained. (i) In first series, basalt tuff was boiled in 3M HNO_3 at a ratio of solid phase:solution = 1:2 for 0.25, 0.5, 0.75, 1.0, 1.5, and 3 h. Samples were washed to a negative reaction to a nitrate ion and dried to constant weight at 110°C. Designation of samples (H-BT-τ, where τ = 0.5, 1.0, 1.5, 3 h). (ii) The second series of samples was obtained by boiling basalt tuff for 0.5 h in a 3M solution of the corresponding acids: HNO_3, H_3PO_4, H_2SO_4 and $C_6H_8O_7$ (citric acid). Legend H$\bar{\text{X}}$–BT-0.5 (H$\bar{\text{X}}$ = HNO_3, H_3PO_4, H_2SO_4 and $K_6H_8O_7$). Samples K_2PdCl_4–$Cu(NO_3)_2$–KBr/$\bar{\text{S}}$ ($\bar{\text{S}}$–H-BT-τ, H$\bar{\text{X}}$–BT-0.5) were prepared by incipient wetness impregnation of each natural basalt tuff with an aqueous solution at certain ratios of the anchored compounds. The wet mass obtained was kept in a closed Petri dish at 20–25°C for 24 h and then dried in an oven at 110°C until constant weight. Palladium(II), copper(II) and KBr contents in the samples thus obtained were 2.72×10^{-5}, 5.90×10^{-5} and 1.02×10^{-4} mol/g, respectively. The catalyst samples were denoted as Pd(II)–Cu(II)/$\bar{\text{S}}$ ($\bar{\text{S}}$ — acid-modified basalt tuff of the first or second series). The samples (10 g) of K_2PdCl_4–$Cu(NO_3)_2$–KBr/$\bar{\text{S}}$ compositions were tested in a gas-flow setup with a fixed-bed glass reactor at an initial CO concentration in the gas-air mixture (GAM), C_{CO}^{in} of 300 mg/m^3 and the following GAM parameters: temperature of 20°C, relative humidity Rh of 67%, a volume flow rate w of 1 L/min, a linear velocity U of 4.2 cm/s. By monitoring final CO concentrations C_{CO}^{f}, a carbon monoxide conversion η [%] was determined as

$$\eta = \frac{(C_{CO}^{in} - C_{CO}^{f})}{C_{CO}^{in}} \times 100\%, \tag{2}$$

where C_{CO}^{in} and C_{CO}^{f} are the initial and final CO concentrations [mg/m^3], respectively. In a steady state mode, η_{st} serves as a parameter characterizing the catalytic activity of the compositions. Taking into account the first order of the reaction with respect to CO and the course of the process in the kinetic region, for the stationary sections of the kinetic curves, the reaction rate constant [s^{-1}] was found. It is given by

$$k_I = \frac{1}{\tau'} \ln\left(\frac{C_{CO}^{f}}{C_{CO}^{in}}\right), \tag{3}$$

where τ' — the effective time [s] for the contact of the gas-air mixture with the catalyst, calculated as the ratio of the height of the catalyst layer to the linear velocity of the gas-air mixture [20].

3. Results and discussion

3.1. Phase compositions

The diffraction patterns of samples N-BT, H-BT-0.5 and Pd(II)–Cu(II)/H-BT-0.5 are shown in Fig. 1a–c, as an example. It can be seen that all

TABLE I

X-ray spectral parameters for natural and modified forms of basalt tuff.

Composition	Phase Mont				Phase Cli		
	d_{001} [Å]	Δd [Å]	d_{006} [Å]	D [nm]	d_{020} [Å]	Δd [Å]	D [nm]
N-BT	14.869	5.269	1.500	26.7	8.955	–	118.0
H-BT-0.5	14.824	5.224	1.502	18.4	8.950	−0.005	117.3
H-BT-1.0	14.713	5.113	1.500	18.2	8.960	+0.005	115.0
H-BT-1.5	14.691	5.091	1.489	17.9	8.941	−0.014	114.3
H-BT-3.0	14.685	5.085	1.497	17.6	8.965	+0.010	114.0
Pd(II)–Cu(II)/N-BT	14.569	4.969	1.500	20.1	8.942	−0.013	117.1
Pd(II)–Cu(II)/H-BT-0.5	14.899	5.299	1.501	12.4	8.988	+0.038	86.0

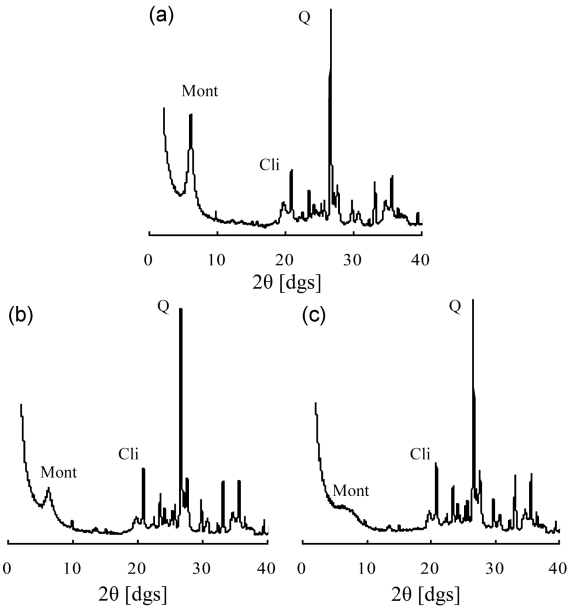

Fig. 1. X-ray diffraction patterns of samples N-BT (a), H-BT-0.5 (b) and Pd(II)–Cu(II)/H-BT-0.5 (c).

samples are crystalline. On the diffraction pattern of the N-BT sample, reflections were identified (only the three most intense reflections are represented) from the following phases layered aluminosilicate:

- montmorillonite (Mont), d = 14.8645, 4.461, 1.500 Å;
- clinoptilolite (Cli), d = 8.988; 3.941; 2.996 Å;
- mordenite (Mord), d = 4.055, 3.785 Å;
- α-quartz (Q), d = 4.266, 3.352, 1.821 Å;
- hematite (α-Fe_2O_3), d = 3.667, 2.261, 1.452 Å.

When processing samples of N-BT with nitrate acid (3M), the intensity of the first basic reflection of the Mont phase (Fig. 1b) decreases markedly in diffractograms, and when palladium(II) and copper(II) salts are applied amorphization of this phase is enhanced (Fig. 1c). Table I shows the position of the reflections d_{001} and d_{006} for the Mont phase and the position of the first base reflection (d_{020}) for the Cli phase. Taking into account the values of d_{001} Mont and the thickness of the aluminosilicate package, we calculated the values of Δd (d_{001} = 9.6 Å), which characterize the distance between the layers.

It can be seen that Δd decreases with increasing contact time of the acid with the N-BT sample, which indicates the replacement of metal cations in the interlayer space with smaller protons. Although the crystallite size (calculated according to the Scherrer formula) of the Mont phase decreases, the crystal structure does not deteriorate (the value of d_{006} is almost constant). When the metal complex composition is applied to N-BT, the interlayer space is compressed, which indicates the localization of the catalyst components on the outer surface of the carrier.

In the case of the Pd(II)–Cu(II)/H-BT-0.5 sample, the Δd parameter increases, the expansion occurs due to the entry of the catalyst components into the interlayer space. Judging by the value of d_{020}, the clinoptilolite phase in the studied samples is almost not subject to structural changes. With an increase in contact time, the deviation of Δd in comparison with N-BT is 0.005–0.01 Å. In the case of the Pd(II)–Cu(II)/H-BT-0.5 sample, we can speak of a slight expansion of the zeolite cell (see Table I).

Modification of the carrier is accompanied by a decrease in the crystallite sizes of the Mont and Cli phases. No significant structural changes were found for the Mord, Q, and hematite phases. For samples of the second series H$\bar{X}$-BT-0.5 (H$\bar{X}$ = HNO_3, H_3PO_4, H_2SO_4 and $K_6H_8O_7$), the X-ray spectral characteristics are independent of the nature of the acid and are almost the same as for sample 3HNO_3–BT-0.5 (Fig. 1, Table I). Heterogenized catalysts are well dispersed, the formation of phases of metal salts, their oxide (PdO, CuO, Cu_2O) and reduced forms (Pd°, Cu°) are not observed.

3.2. Morphology

The morphology of basalt tuff is not described in the available literature. We presented SEM images of the scattering of particles of an averaged fraction (not more than 0.75 mm) of N-BT, 3H-BT-0.5 and Pd(II)–Cu(II)/H-BT-0.5 (Fig. 2) samples.

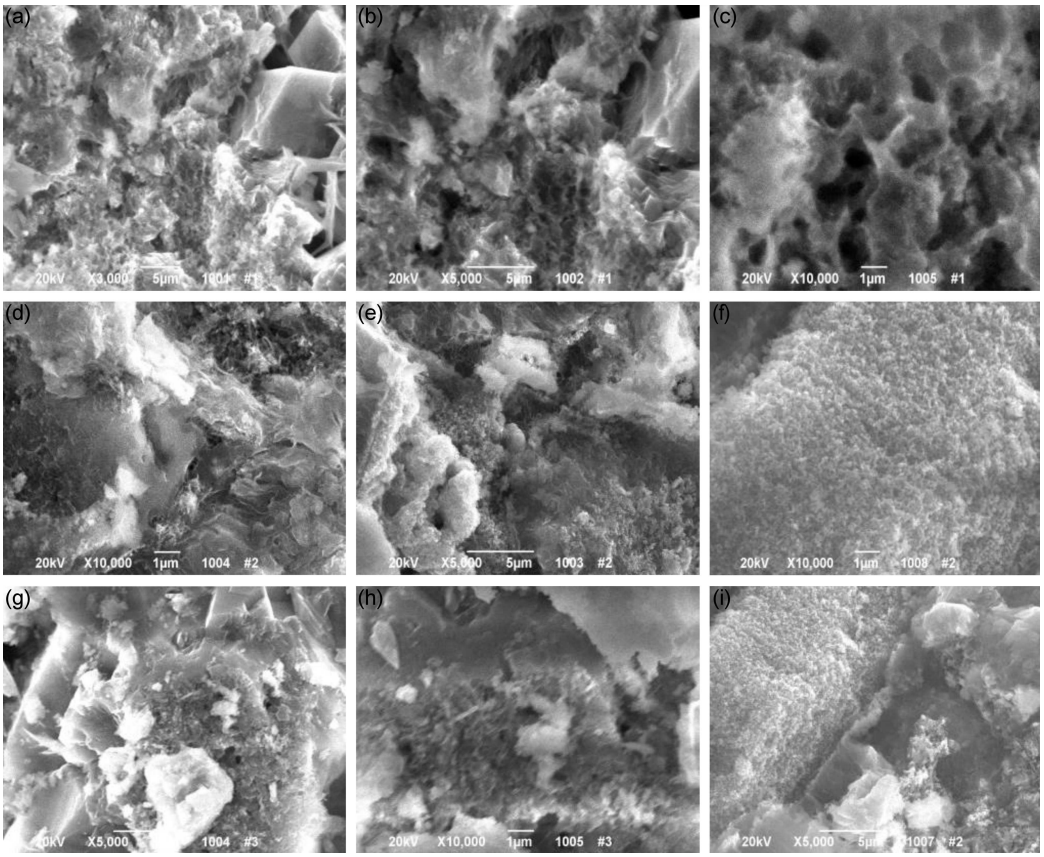

Fig. 2. SEM images of particle of N-BT samples (a–c); 3H-BT-0.5 (d–f); Pd(II)–Cu(II)/H-BT-0.5 (g–i).

According to XRD data, the dominant phases are Mont, Cli and Mord. Each phase is characterized by its morphological characters, which are well described in the literature [35–37]. It can be seen in Fig. 2a–c that various morphotypes are found in the samples: large-block crystals of clinoptilolite, lamellar and coarse-cell structure of montmorillonite, filiform crystals of mordenite that come into contact with the phases Mont and Cli. Even with short-term processing of 3M HNO_3 basaltic tuff, some morphological changes are observed (Fig. 2d–f), such as condensation of agglomerates while maintaining the coarse-cellular structure of Mont and interwoven thin filaments of the Mord phase. There is also an agglomeration of closely adjacent shapeless fine particles (Fig. 2f), which are the result of the action of nitric acid on the surface of large-block clinoptilolite crystals.

When applying palladium(II) and copper(II) salts, the surface morphology does not change significantly (Fig. 2g–i). The formation of new phases due to the components of the catalyst is not observed. Large-sheet crystallites and agglomerates formed by decompressed (loose) shapeless fine particles are visible. It is characteristic for the nature of the acid that the morphological picture of the second series of 3H-BT-0.5 samples remains almost unchanged, which is due to the relatively mild conditions for processing the carrier.

3.3. FT-IR spectroscopy

Figure 3 shows the FT-IR spectra of samples N-BT, H-BT-0.5, and Pd(II)–Cu(II)/H-BT-0.5, which are typical for aluminosilicate minerals [23–27]. We will therefore comment on only one band. A very strong band at 1020 cm^{-1} refers to the internal asymmetric stretching vibrations of the main structural units of the SiO_4 and AlO_4 tetrahedra or the Si–O–Si and Si–O–Al bridges.

This band is very wide, and the shoulder at 1150 cm^{-1} is clearly distinguished for N-BT, which is sensitive to structural changes [26]. Judging by our data, it disappears as a result of acid modification of N-BT, which may indicate a decrease in the crystallinity of the samples. This is confirmed by the data of the ray phase analysis. The position and shape of the band at 1020 cm^{-1} depend on a number of factors. Thus, during the acid treatment of N-BT samples, it shifts to the region of high wave numbers, which indicates a decrease in the number of aluminum atoms in the structure of the zeolite framework, resulting from acid dealumination [27].

3.4. Protolytic properties

It is known that the interaction of water molecules with the surface of natural and modified aluminosilicates is accompanied by the formation of an acidic or alkaline environment. Changes in

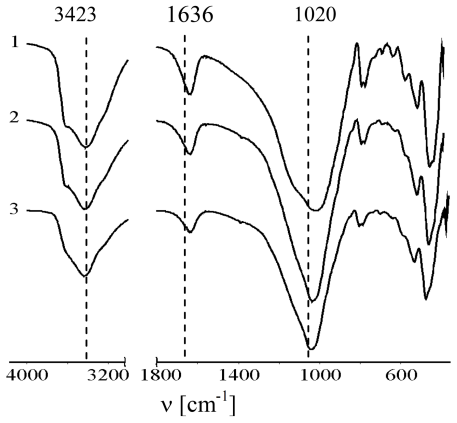

Fig. 3. FT-IR spectra of samples of natural and chemically modified basalt tuff: N-BT (curve 1), H-BT-0.5 (curve 2), Pd(II)–Cu(II)/H-BT-0.5 (curve 3).

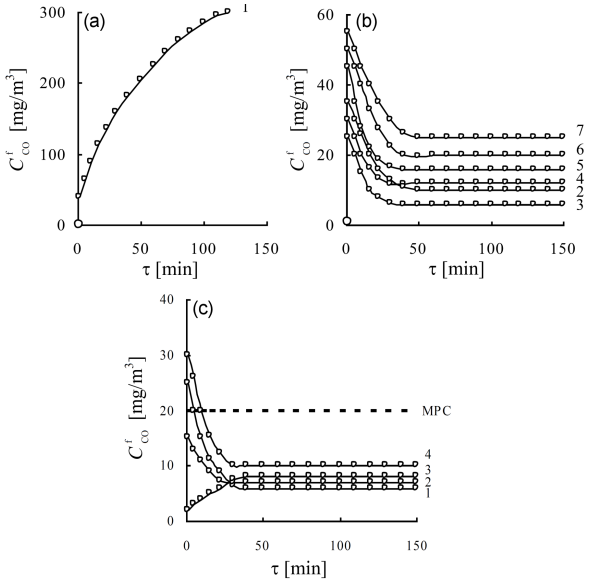

Fig. 4. The change in C^{f}_{CO} over time during the oxidation of carbon monoxide by oxygen in the presence of a catalyst K_2PdCl_4–$Cu(NO_3)_2$–KBr/$\bar{S}$ (a) $\bar{S}$ = N-BT (1); (b) $\bar{S}$ = H-BT-τ, where τ = 0.25 h (2); 0.5 h (3); 0.75 h (4); 1.0 h (5); 1.5 h (6); 3.0 h (7); (c) $\bar{S}$ = H$\bar{X}$-BT-0.5; H$\bar{X}$: HNO_3 (1), H_3PO_4 (2), $C_6H_8O_7$ (3) and H_2SO_4 (4).

the pH of the suspension of the studied samples showed that the equilibrium pH values (pH_S) are quickly established (in no more than 15–20 min) and depend on the processing conditions of basalt tuff. For the first series of H-BT-samples, with increasing contact time of the acid with the sample, the pH_S decreases: N-BT (6.50) > H-BT-0.25 (5.50) > H-BT-0.5 (5.20) > H-BT-0.75 (5.0) > H-BT-1.0 (4.90) > H-BT-1.5 (4.80) > H-BT-3.0 (4.70). The greatest decrease in pH of the suspension occurs upon contact of 0.25 and 0.5 h. A further increase in contact time (4 times) leads to a decrease in pH by only 0.3 pH units. For the second series of samples H$\bar{X}$-BT-0.5, lowering the pH of the suspension depends on the nature of the acid: N-BT (6.50) > $C_6H_8O_7$-BT 0.5 (5.55) > HNO_3-BT-0.5 (5.20) > H_3PO_4-BT-0.5 (4.28) > H_2SO_4-BT-0.5 (4.03). Thus, acid-modified samples are characterized by lower pH_S values, which significantly affects the composition of surface palladium–copper complexes [3, 17, 22].

3.5. Testing of Pd(II)–Cu(II)-catalysts in the oxidation of CO with oxygen

Figure 4 shows the kinetic curves of the change in the final concentration of CO (C^{f}_{CO}) over the time of three series of catalysts. In the first catalyst, the initial basalt tuff acts as a carrier (Fig. 4a) In the second series of catalysts, samples of modified boiling 3M HNO_3 basaltic tuff were used at different contact times of H-BT-τ (Fig. 4b). In the third series, samples modified with different acids (3M) for 0.5 h were used as a carrier (Fig. 4c).

It can be seen from the presented results that the metal complex composition deposited on the initial basalt tuff does not exhibit catalytic properties — C^{f}_{CO} increases in time and reaches an initial concentration of C^{in}_{CO} = 300 mg/m^3 (Fig. 4a). However, when the 3M HNO_3 carrier is processed even for 0.25 h (Fig. 4b, curve 2), the properties of the catalytic system change sharply: the CO concentration at the output of the reactor decreases for about 30 min and then remains constant for a long time (C^{f}_{CO} = 10 mg/m^3). With an increase in BT pretreatment time, the kinetic curve profiles do not change, however, the maximum catalytic activity of the samples (C^{f}_{CO} = 6 mg/m^3, η_{st} = 98%) is observed in the case of an H-BT-0.5 carrier. In the case of using carrier H-BT-3, the catalyst does not provide the conversion of CO to maximal permissible concentration (MPC), i.e, $C^{f}_{CO} > MPC_{CO}$ (Fig. 4b, curve 7). Figure 4c demonstrate the kinetics of CO oxidation with oxygen in the presence of K_2PdCl_4-$Cu(NO_3)_2$-KBr/H$\bar{X}$-BT-0.5 catalysts. Carriers were treated with nitrate acid (curve 1), phosphate (curve 2), citric (curve 3), and sulfate (4) acids. It can be seen that regardless of the nature of the acid, under the same conditions of carrier modification, the catalysts oxidize CO below the MPC in a stationary mode (C^{f}_{CO} values are in the range of 6–10 mg/m^3). It should be noted that in the case of treatment of the carrier with citric acid, the profile of the kinetic curve differs from the others within 40 min. Namely, C^{f}_{CO} increases from 2 mg/m^3 at the beginning of the experiment to 8 mg/m^3 in a stationary mode. The change (increase or decrease) in the activity of the palladium–copper catalyst in the initial period of the reaction, which the authors also noted [7, 27], is due to different mechanisms of the formation of intermediate catalytically active forms of palladium(II) and copper(II) [8, 11, 15].

TABLE II

Effect of the pH suspension of acid-modified samples on the activity of K_2PdCl_4–$Cu(NO_3)_2$–KBr/$\bar{S}$ by CO oxidation catalysts with oxygen.

Carrier ($\bar{S}$)	pH_S	C^f_{CO} [mg/m^3]	η_{st} [%]	k_I [s^{-1}]
N-BT	6.5	300	–	–
H-BT-0.25	5.5	10	97	6.54
H-BT-0.5	5.2	6	98	7.52
H-BT-0.75	5.0	12	96	6.19
H-BT-1.0	4.9	16	95	5.64
H-BT-1.5	4.8	20	93	5.21
H-BT-3.0	4.7	25	92	4.78
HNO_3-BT-0.5	5.2	6	98	7.52
H_3PO_4-BT-0.5	4.3	7	98	7.23
$C_6H_8O_7$-BT-0.5	5.6	8	97	6.97
H_2SO_4-BT-0.5	4.0	10	97	6.54

Taking into account all the data obtained, it can be concluded that under conditions of gentle (soft) acid modification, the crystalline structure is mainly preserved. However, especially in the case of a catalyst, crystallite sizes are reduced, and aggregated particles decompress. Under the influence of acid, ion-exchange processes and dealumination of the aluminosilicate framework are carried out, as a result of which protolysis is enhanced, and the pH of the layer of water molecules adsorbed by the carrier decreases. It has been shown in many of our studies [3, 17–22] that catalytically active palladium–copper complexes, depending on the nature of the support, form in a wide pH range, which is due to the variety of complex forms of palladium(II) and copper(II). Table II summarizes data on the effect of the pH of the suspension on some parameters (C^f_{CO}, η_{st}, k_I is the first-order constant by CO) of the oxidation of carbon monoxide by oxygen in the stationary mode in the presence of the K_2PdCl_4–$Cu(NO_3)_2$–KBr/$\bar{S}$ catalyst. It can be seen that for the first series of samples ($\bar{S}$ = H-BT-τ) with a decrease in pH from 6.5 to 4.7, the maximum value of the constant k_I is reached at pH 5.2, when the contact time of the sample with acid is 0.5 h. In this case, C^f_{CO} reaches a minimum value. It should be noted that in this series all catalyst samples, except H-BT-3, provide such a degree of CO conversion at which $C^f_{CO} \leq MPC_{CO}$. For BT samples of the second series, pH_S depends on the nature of the acid and varies from 5.6 to 4.0 (the lowest pH value is observed in the case of modification with sulfate acid). Although the tendency for the reaction parameters to change is the same as in the first series, in the pH range from 4.0 to 5.6, these differences are not as significant as in the first series.

It should be noted that the catalytic activity of the presented samples and those described in the literature [20, 28, 29] differs little in the stationary mode (the CO conversion rate is 93–98%). Significant differences in catalytic activity are observed at the initial stage of the reaction. For known catalysts, the condition $C^f_{CO} < MPC_{CO}$ is reached within 40–50 min [20]. New catalysts do not have this drawback.

4. Conclusions

Catalysts K_2PdCl_4–$Cu(NO_3)_2$–KBr/$\bar{S}$ were obtained containing, as carriers, basalt tuff modified with boiling 3M HNO_3 at different contact times (H-BT-τ, where τ = 0.25; 0.5; 0.75; 1.0; 1.5; 3 h), and modified with various acids (H$\bar{X}$-BT-0.5; H$\bar{X}$ = HNO_3, H_3PO_4, H_2SO_4, $C_6H_8O_7$). Carriers and catalysts are characterized by XRD, FT-IR, and pH metering. Natural basalt tuff (N-BT) is a polyphase mineral in which the phases of montmorillonite, clinoptilolite, mordenite, α-quartz and goethite predominate. After acid treatment and deposition of the catalyst components, the phase composition does not change, however, the crystallite size of the Mont and Cli phases decreases. Due to the substitution of metal cations by hydrogen ions and dealumination of the support, the acid properties of the surface change the pH of the suspension, which decreases from 6.5 to 4.0. The catalyst samples were tested in the reaction of low-temperature oxidation of carbon monoxide by atmospheric oxygen. It has been shown that the maximum activity of the catalyst Pd(II)–Cu(II)/$\bar{S}$ is observed when $\bar{S}$ = H-BT-0.5. In all cases, except for $\bar{S}$ = H-BT-3, in a stationary mode, the concentration of CO at the output of the reactor is less than the maximum permissible concentration for the working zone (20 mg/m^3). For samples of the second series ($\bar{S}$–H$\bar{X}$-BT-0.5), the nature of the acid almost does not affect the degree of CO conversion in the stationary mode. However, in the case of basalt tuff modification with citric acid, the kinetics of CO oxidation changes, i.e., C^f_{CO} increases at the initial stage and the stationary mode is reached at $C^f_{CO} < MPC_{CO}$.

References

[1] W.G. Lloyd, D.R. Rowe, *Environ. Sci. Technol.* **3**, 1133 (1971).

[2] W.G. Lloyd, D.R. Rowe, US Patent US3790662A, Palladium Compositions Suitable as Oxidation Catalysts, 1974.

[3] T.L. Rakitskaya, A.A. Ennan, V.Y. Volkova, *Low-Temperature Catalytic Air Purification from Carbon Monoxide*, Ekologiya, Odessa 2005 (in Russian).

[4] T.L. Rakitskaya, T.A. Kiose, A.A. Ennan, V.Ya. Volkova, A.M. Djiga, K.O. Golubchik, *Odesa Nat. Univ. Herald. Chem.* **18**, 5 (2013).

[5] K.D. Kim, I.-S. Nam, J.S. Chung, J.S. Lee, S.G. Ryu, Y.S. Yang, *Appl. Catal. B: Environ.* **5**, 103 (1994).

[6] D.J. Koh, J.H. Song, S.W. Ham, I.S Nam, *Kor. J. Chem. Eng.* **14**, 486 (1997).

[7] E.D. Park, J.S. Lee, *J. Catal.* **180**, 123 (1998).

[8] L. Bruk, D. Titov, A. Ustyugov et al., *Nanomaterials* **8**, 217 (2018).

[9] Y. Yamamoto, T. Matsuzaki, K. Ohdan, Y. Okamoto, *J. Catal.* **161**, 577 (1996).

[10] E.D. Park, J.S. Lee, *J. Catal.* **193**, 5 (2000).

[11] E.D. Park, S.H. Choi, J.S. Lee, *J. Phys. Chem. B* **104**, 5586 (2000).

[12] L. Wang, Y. Zhang, Y. Lou, Ya. Guo, G. Lu, Yu. Guo, *Fuel Process. Technol.* **122**, 23 (2014).

[13] M.N. Desai, J.B. Butt, J.S. Dranoff, *J. Catal.* **79**, 95 (1983).

[14] V.Z. Radkevich, K. Wilson, S.G. Khaminet, T.L. Sen'ko, *Kinet. Catal.* **55**, 252 (2014).

[15] S.G. Haminec, V.Z. Radkevich, K. Vil'son, T.L. Sen'ko, *Proc. Natl. Acad. Sci. Belarus, Chem. Ser.* **4**, 37 (2014).

[16] F. Zhou, X. Du, J. Yu, D. Mao, G. Lu, *RSC Advances* **6**, 66553 (2016).

[17] T.L. Rakitskaya, V.Ya. Paina, A.A. Ennan, *Russ. J. Coord. Chem.* **13**, 1393 (1987).

[18] T.L. Rakitskaya, T.A. Kiose, A.G. Voloschuk, L.P. Oleksenko, V.Ya. Volkova, L.I. Reznik, *Russ. J. Appl. Chem.* **82**, 204 (2009).

[19] T.L. Rakitskaya, T.A. Kiose, A.A. Ennan, K.O. Golubchik, L.P. Oleksenko, V.G. Gerasiova, *Russ. J. Phys. Chem.* **90**, 6 (2016).

[20] T.L. Rakitskaya, T.A. Kiose, K.O. Golubchik, A.A. Ennan, V.Y. Volkova, *Chem. Cent. J.* **11**, 28 (2017).

[21] T.L. Rakitskaya, T.A. Kiose, A.M. Zryutina, R.E. Gladyshevskii, A.S. Truba, V.O. Vasylechko, P.Yu. Demchenko, G.V. Gryschouk, V.Ya. Volkova, *Solid State Phenom.* **200**, 299 (2013).

[22] T.L. Rakitskaya, G.M. Dzhyga, T.A. Kiose, L.P Oleksenko, V.Y. Volkova, *SN Appl. Sci.* **1**, 291 (2019).

[23] A. Ates, C. Hardacre, *J. Colloid Interface Sci.* **372**, 130 (2012).

[24] P. Ambrozova, J. Kynicky, T. Urubek, V.D. Nguyen, *Molecules* **22**, 1107 (2017).

[25] G.E. Christidis, D. Moraetis, E. Keheyan, L. Akhalbedashvili, N. Kekelidze, R. Gevorkyan, H. Yeritsyan, H. Sargsyan, *Appl. Clay Sci.* **24**, 79 (2003).

[26] M.S. Joshi, V.V. Joshi, A.L. Choudhari, M.W. Kasture, *Mater. Chem. Phys.* **48**, 160 (1997).

[27] F. Cakicioglu-Ozkan, S. Ulku, *Micropor. Mesopor. Mater.* **77**, 47 (2005).

[28] T. Rakitskaya, G. Dzhyga, T. Kiose, V. Volkova, in: *Nanooptics and Photonics, Nanochemistry and Nanobiotechnology, and Their Applications*, Vol. 247, Eds. O. Fesenko, L. Yatsenko, Springer, Cham 2020, p. 141.

[29] T.L. Rakitskaya, T.A. Kiose, A.A. Ennan, *Odesa Nat. Univ. Herald. Chem.* **25**, 6 (2020).